Ecological Indicators 130 (2021) 108075

Contents lists available at ScienceDirect

Ecological Indicators

journal homepage: www.elsevier.com/locate/ecolind

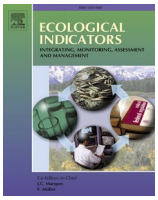

Changes in global climate heterogeneity under the 21st century global warming

Yanlong Guan [a,b,c], Hongwei Lu [a,b,*], Yelin Jiang [e], Peipei Tian [a,b], Lihua Qiu [b], Petri Pellikka [c,d], Janne Heiskanen [c,f]

[a] Key Laboratory of Water Cycle and Related Land Surface Process, Institute of Geographic Science and Natural Resources Research, Chinese Academy of Science, Beijing, China
[b] School of Renewable Energy, North China Electric Power University, Beijing, China
[c] Department of Geosciences and Geography, University of Helsinki, Finland
[d] State Key Laboratory for Information Engineering in Surveying, Mapping and Remote Sensing, Wuhan University, Wuhan 430079, China
[e] Department of Civil and Environmental Engineering, University of Connecticut, Storrs, CT, USA
[f] Institute for Atmospheric and Earth System Research, Faculty of Science, University of Helsinki, Finland

ARTICLE INFO

Keywords:
Climate diversity
Köppen–Geiger climate classification
Landscape
CMIP5
SHDI
SIDI

ABSTRACT

Variations in climate types are commonly used to describe changes in natural vegetation cover in response to global climate change. However, few attempts have been made to quantify the heterogeneous dynamics of climate types. In this study, based on the Coupled Model Intercomparison Project phase 5 (CMIP5) historical and representative concentration pathway (RCP) runs from 18 global climate models, we used Shannon's Diversity Index (SHDI) and Simpson's Diversity Index (SIDI) to characterise of global climate heterogeneity from a morphological perspective. Our results show that global climate heterogeneity calculated by the SHDI/SIDI indices decreased from 1901 to 2095 at a significance level of 0.01. As radiative forcing intensified from RCP 2.6 to 8.5, the SHDI/SIDI decreased significantly. Furthermore, we observed that the spatial distribution of global climate heterogeneity was significantly reduced, with a pronounced latitudinal trend. Sensitivity analysis indicated that the temperature increase played a more significant role in reducing global climate heterogeneity than precipitation under the three warming scenarios, which is possibly attributed to anthropogenic forcing. Our findings suggest that the dynamics of global climate heterogeneity can be an effective means of quantifying global biodiversity loss.

1. Introduction

The relationships between climate change and other ongoing human-induced threats (such as loss of natural habitats) are expected to present serious challenges for biodiversity in the 21st century. To effectively manage and protect natural resources, it is necessary to accurately predict the potential impact of climate change on biodiversity (Gaston, 2000; Deutsch et al., 2008; Elsen et al., 2018). To address this issue, researchers have developed a series of bioclimatic models to measure the relationships between individual species and climate change through statistical or process analysis (Guisan and Zimmermann, 2000; Niskanen et al., 2017). In these models, climatic factors are generally considered to be the main driving force determining the spatial distribution of species (Sunday et al., 2012; Beck et al., 2018). However, because most species on Earth lack sufficient population or physiological data, it is difficult to construct accurate models or predictions. An alternative approach is to use simpler indicators of climate change to quantify and explain the different threats and opportunities for ecosystems or biodiversity (Ohlemüller et al., 2008; Beaumont et al., 2011; Burrows et al., 2011; Garcia et al., 2014).

Climatic indicators expressed as isotherm shifts or a mixture of temperature and precipitation indices vary across space and time, as described in previous studies (Ohlemüller et al., 2008; Vicente-Serrano et al., 2010; van der Schrier et al., 2013; Schwalm et al., 2017; Mahony and Cannon, 2018). However, these climatological indicators do not necessarily characterise biomes. Given that multi-year vegetation

* Corresponding author at: Key Laboratory of Water Cycle and Related Land Surface Process, Institute of Geographic Science and Natural Resources Research, Chinese Academy of Science, Beijing, China.
E-mail address: luhw@igsnrr.ac.cn (H. Lu).

https://doi.org/10.1016/j.ecolind.2021.108075
Received 23 July 2020; Received in revised form 14 July 2021; Accepted 2 August 2021
Available online 5 August 2021

coverage is considered to be 'visible climate', the Köppen–Geiger climate scheme is commonly used to describe global biome distributions (Wang and Overland, 2004; Beck et al., 2018). The strong correspondence between climate and biome types allows the Köppen–Geiger criteria to be used across numerous applications. The Köppen–Geiger climate classification based on the threshold values and seasonality of monthly air temperatures and precipitation as an indicator of vegetation coverage was initially summarised by Köppen (1931). Since then, it has been modified into different versions (Lee, 1947; Thornthwaite, 1948; 1961; Feddema, 2005; Kottek et al., 2006; Peel et al., 2007).

The availability of recently observed and simulated grid datasets allows for the diagnosis or prediction of climate change by exploring the changing climate type boundaries across time and space. For example, Seidel et al. (2008) indicated that the tropical climate type has expanded since the 1970 s. Feng et al. (2012) reported that the climate types in 31.3%–46.3% of global land area are estimated to change by the end of this century under RCP4.5 and RCP8.5 scenarios. Mahlstein et al. (2013) revealed that the pace of shifts in global climate types under RCP 8.5 is significantly related to the temperature increase. Chan and Wu (2015) demonstrated that approximately 5.7% of Earth's surface has become drier and hotter. They attributed these changes to anthropogenic activities that have occurred since 1950. Lu et al. (2020) revealed patch aggregation effects accompanied by changes in the global climatic landscape. Despite the widespread use of Köppen metrics in previous studies, we still have a limited understanding of how the global climate system maintains its heterogeneity, that is, the diversity and complexity of the spatial distribution of climate type changes. For example, as the temperature rises, cold climates (such as tundra, frost, or alpine climates) in the Arctic and major mountainous regions of the world tend to shrink, while tropical and arid warm climates (such as savannah or desert climates) expand. These global complementary changes are likely to lead to changes in climate heterogeneity. The strong spatial overlap between climate and biome types makes climate heterogeneity for explaining the potential impact of climate change on biodiversity.

The global climatic landscape consists of different patches with various climatic hydrothermal conditions (Pickett and Cadenasso, 1995). Spatial morphology allows the use of a landscape index to describe heterogeneous changes in the climatic landscape (Guan et al., 2020). These morphological measurements are predominantly based on the assumption that the spatial heterogeneity of climatic conditions has a significant impact on the distribution of spatial vegetation or ecosystems (Garcia et al., 2014). In particular, many species are heavily dependent on different climate types, particularly in their key phases of life, such as migration, growth, and reproduction. Previous research (Guan et al., 2020) has revealed that morphological changes in the climate landscape could be an important indicator of climate change. However, recent studies have shown that the spatial heterogeneity of climate itself has not attracted widespread attention in different warming scenarios (Taylor et al., 2012). We hypothesise that the decrease of climate heterogeneity will lead to the homogenization of the eco-climatic zones, which may further limit the speciation and migration of species, and reduce the biodiversity at a given spatial scale.

This study aimed to detect the spatiotemporal characteristics of global-scale climate heterogeneity. Owing to the overlapping spatial relationships between climate and vegetation, the dynamics of global climate heterogeneity can provide insight into global biodiversity changes. First, we identified the changes in the main climate type area under different warming scenarios to quantify the impact of different emission pathways on the climatic landscape. Subsequently, we used the diversity index to identify the heterogeneity of spatiotemporal features from the perspective of spatial morphology. We then used a sensitivity analysis to distinguish the effects of temperature and precipitation on climate heterogeneity. Finally, we analysed the impacts of different model data uncertainties on the climate heterogeneity calculations. Exploring global climate heterogeneity stands to provide a useful reference for identifying and predicting future changes in biodiversity.

2. Materials and methods

2.1. Climate data and pre-treatments

We collated global monthly land simulated temperature and precipitation gridded datasets (excluding Antarctica) derived from multiple coupled atmosphere–ocean global climate models (GCMs), dividing them into four periods: P1 (1901–1950), P2 (1951–2000), P3 (2001–2050), and P4 (2051–2095). These GCM simulations were collected from the historical and RCP 2.6, 4.5, and 8.5 runs from the Coupled Model Intercomparison Project phase 5 (CMIP5) (https://esgf-node.llnl.gov/search/cmip5/), as established by the World Climate Research Programme (Taylor et al., 2012).

The RCP emission scenarios offer different projections of future anthropogenic climate changes (Taylor et al., 2012). This provides an opportunity to explore responses over a range of warming trends from low to high. Specifically, the RCP 2.6, 4.5, and 8.5 emissions pathways correspond to the estimated minimum, medium, and maximum added mean radiative forcing (~2.6, 4.5, and 8.5 W/m^2, respectively, relative to pre-industrial conditions) by the end of this century. In the CMIP5 design process, the initialisation conditions for each model are sensitive to different methods or observational datasets (Taylor et al., 2010). To maintain consistency in the results of the models, similar to those of Mahlstein et al. (2013) and Lu et al. (2019), we used the same ensemble (r1i1p1) from the 18 typical models (Table S1), and all simulations were interpolated to regular $1^\circ \times 1^\circ$ grid boxes by bilinear interpolation to maintain the same resolution.

Furthermore, we used the nine model outputs (Table S2) provided by the CMIP5 historical single-forcing experiments that were driven by natural forcing only (HIST-NAT), greenhouse gas forcing only (HIST-GHG), and combined forcing (HIST-ALL). Because the historical attribution experiment lasted until 2006, we selected 1940–2006 as a typical period to illustrate the different effects of natural variation and anthropogenic forcing. Specifically, the HIST-NAT simulations were driven by natural forcing only (e.g. volcanoes and solar variability) evolving in the control run. These simulations further featured fixed pre-industrial conditions, such as prescribed atmospheric concentrations of some short-lived species and prescribed non-evolving emissions of natural aerosols and unperturbed land use. Similar to the imposed conditions of NAT, the HIST-GHG simulations were driven by greenhouse gas forcing only (consistent with observations) evolving in the control run under fixed natural forcing. The HIST-ALL simulations were driven by a combination of anthropogenic forcing, natural forcing, and land-use changes. In comparison, the contribution of HIST-GHG or HIST-NAT experiments to recent climate zone changes can be distinguished from the estimates of HIST-ALL. Similar to the above-mentioned analysis, all single-forcing experiment datasets were interpolated to regular $1^\circ \times 1^\circ$ grid boxes by bilinear interpolation to explore the possible causes of global climate heterogeneity.

The Köppen–Geiger scheme can be sensitive to certain thresholds, and models can have difficulty in simulating present-day distributions of the correct Köppen–Geiger climate zones. Therefore, in this study, we followed data pre-treatments previously reported by Mahlstein et al. (2013) and Chan et al. (2016). First, the monthly anomalies for each historical and RCP run from 1980 to 1999 relative to the monthly mean were calculated and then added to the observational 'base period' of the 1980–1999 monthly means to generate the climatological temperature and precipitation datasets. For temperature and precipitation, this results in a time period of 195 years covering 1901–2095. Second, for the climate model outputs of single-forcing experiments, we calculated the observational monthly means for 1940–1969 and added them to the historical monthly anomalies to generate the climatological distribution of temperature and precipitation covering 1940–2000. The observed monthly temperature and precipitation data from 1980 to 1999 and from 1940 to 1969 were provided by the Climatic Research Unit Timeseries (CRU TS) version 3.2. CRU TS supplies a gridded time-series

dataset based on observational records from more than 4,000 sites worldwide. The monthly average surface temperature and precipitation are included as climatological references in this study. This method has been used widely in similar climatic research fields (Mahlstein et al., 2013; Feng et al., 2014; Chan et al., 2016) and is helpful for reducing errors in climate classification. Subsequently, a five-year running mean method was used to increase the robustness of each model's temperature and precipitation datasets because the annual changes may include larger internal climate variability unrelated to climate trends. However, the results are not highly sensitive to time scales in 15yrs (Mahlstein et al., 2013; Chan and Wu, 2015).

2.2. Computing the Köppen–Geiger climate types

The Köppen–Geiger climate classification method (Peel et al., 2007) was employed to separate the global land area into five climate types (the 30 subtypes are not included here) on a grid-scale (Table S3): tropical climate (A), arid climate (B), polar climate (E), temperate climate (C), and cold climate (D). Based on this scheme, each land grid location was assigned a specific climatic code (A–E). In this study, the percentage area change of a specific climate type was calculated based on the change in the number of grid boxes in that climate type.

2.3. Computing climate heterogeneity

The public domain software FRAGSTATS (version 4.2) was used for landscape analyses (McGarigal et al., 2002). It has been widely used in several fields of research, such as landscape ecology. Although FRAGSTATS provides several spatial metrics, many quantify similar or identical aspects of landscape patterns. In most cases, redundant indicators have high correlations, or may even correlate perfectly. Despite these limitations, landscape indices describe different features of landscape patterns, such as shape, structure, and diversity. To reduce the uncertainty of the Köppen map projection, we selected area-based Shannon's Diversity Index (SHDI) and Simpson's Diversity Index (SIDI) to characterise the dynamics of global climate heterogeneity. In general, SHDI (Shannon, 1948) is more sensitive to richness than evenness, whereas SIDI (Simpson, 1949) is the opposite. The SHDI increases with the number of different patch types, and as the distribution of areas among climatic patch types becomes more homogeneous. The SHDI value can be determined as follows:

$$SHDI = -\sum_{i=1}^{I}(p_i \times lnp_i) \quad (1)$$

where p_i is the proportion of the grid boxes occupied by climatic patch types, and I is the number of climatic patch types present in the global climate types ($I = 5$ in this study). This proportion can be estimated as $p_i = N_i/N$, where N_i is the total number of grid boxes belonging to the i-th type.

The SIDI (Figure S1–S5) is another measure of diversity and represents the probability that two grid boxes randomly selected from a climatic sample belong to different climate types. It can be determined as follows:

$$SIDI = 1 - \sum_{i=1}^{I} p_i^2 \quad (2)$$

where p_i is the proportion of grid boxes occupied by the climatic patch types. When the climatic landscape contains only one patch (i.e. no diversity), SIDI = 0. SIDI approaches 1 as the number of different patch types increases and the proportional distribution of area among patch types becomes more even.

2.4. Computing the geographic features of global diversity patterns

For geographic features, we used the moving window and standard deviational ellipse (SDE) methods (Scott and Janikas, 2010) to calculate the spatial distribution of SHDI. First, using the eight-cell neighbourhood rule in the FRAGSTATS 4.2 software platform (McGarigal et al., 2002), we computed the squared SHDI patterns with a minimum side length of 2° over each positively valued grid box and returned a value to the centre grid boxes. To identify the spatial characteristics in the four periods, we used the SDE method from the direction distribution module of ArcGIS 10.0 to generate new fields and features, including standard distances of long and short axes and elliptical polygons. The long semi-axis (Y-standard distance, β) of the ellipse characterises the directional trends of the spatial distribution, and the short semi-axis (X-standard distance, α) represents the spatial distribution range. The shorter the X-standard distance of the SDE, the smaller and more aggregated the spatial distribution coverage.

2.5. Statistical analysis

The Mann–Kendall trend test (Kendall, 1975; Mann, 1945) is a non-parametric trend test that is widely used to assess the significance of meteorological time-series trends. The null hypothesis in the Mann–Kendall test means that the data are independent and randomly ordered. The results of the trend test clarify the magnitude of the correlation and direction of the relationship. The range of the coefficient values was 1 to –1, which indicates positive and negative correlations, respectively. The t-test was used to determine whether the correlation coefficient was significantly different from zero, indicating a correlation between the two variables.

2.6. Sensitivity and uncertainty analysis

Considering temperature and precipitation sensitivities, we first kept the temperature or precipitation constant for each model under the three emission pathways from 1901 to 2095. Then, we simulated the SHDI for each model to distinguish the impacts of temperature and precipitation on variations in global climate heterogeneity. In terms of uncertainty, we first evaluated the differences of all models in the SHDI simulation using a box-and-whisker plot (Zhang et al., 2018), in which the lengths of the interquartile range and whisker reflect the biases of each model to the corresponding multi-model mean. Meanwhile, based on alpha models, the Cronbach alpha (α) coefficient (Bonett and Wright, 2015) was used to check the internal consistency of all models as a whole, meaning that the smaller the Cronbach's alpha coefficient value, the more discrete the interior.

3. Results

3.1. Changes in climate types from the simulation dataset

Figure 1 illustrates that the degree of change in areas for global climate types tends to increase from RCP 2.6 to 8.5. The disappearing types occur mainly at high latitudes and altitudes, especially in Alaska, East Siberia, Tibet, and East Africa. Overall, tropical, arid, and cold climates are expanding, whereas polar climates are decreasing under the three emission pathways. Specifically, Fig. 2 indicates that the cumulative percentage area of tropical climate has increased by 1.17%, 2.00%, and 2.75% in RCP 2.6, 4.5 and 8.5, respectively, in the 1901–1950/2051–2095 comparison periods. The cumulative increases in the arid climate are 1.31%, 1.86%, and 3.44%, respectively. The increases in the cold climate are 1.79%, 1.95%, and 2.26%, respectively. However, the polar climates decrease more rapidly with a cumulative percentage area of –4.15%, –5.35%, and –7.94% from RCP 2.6 to 8.5, respectively.

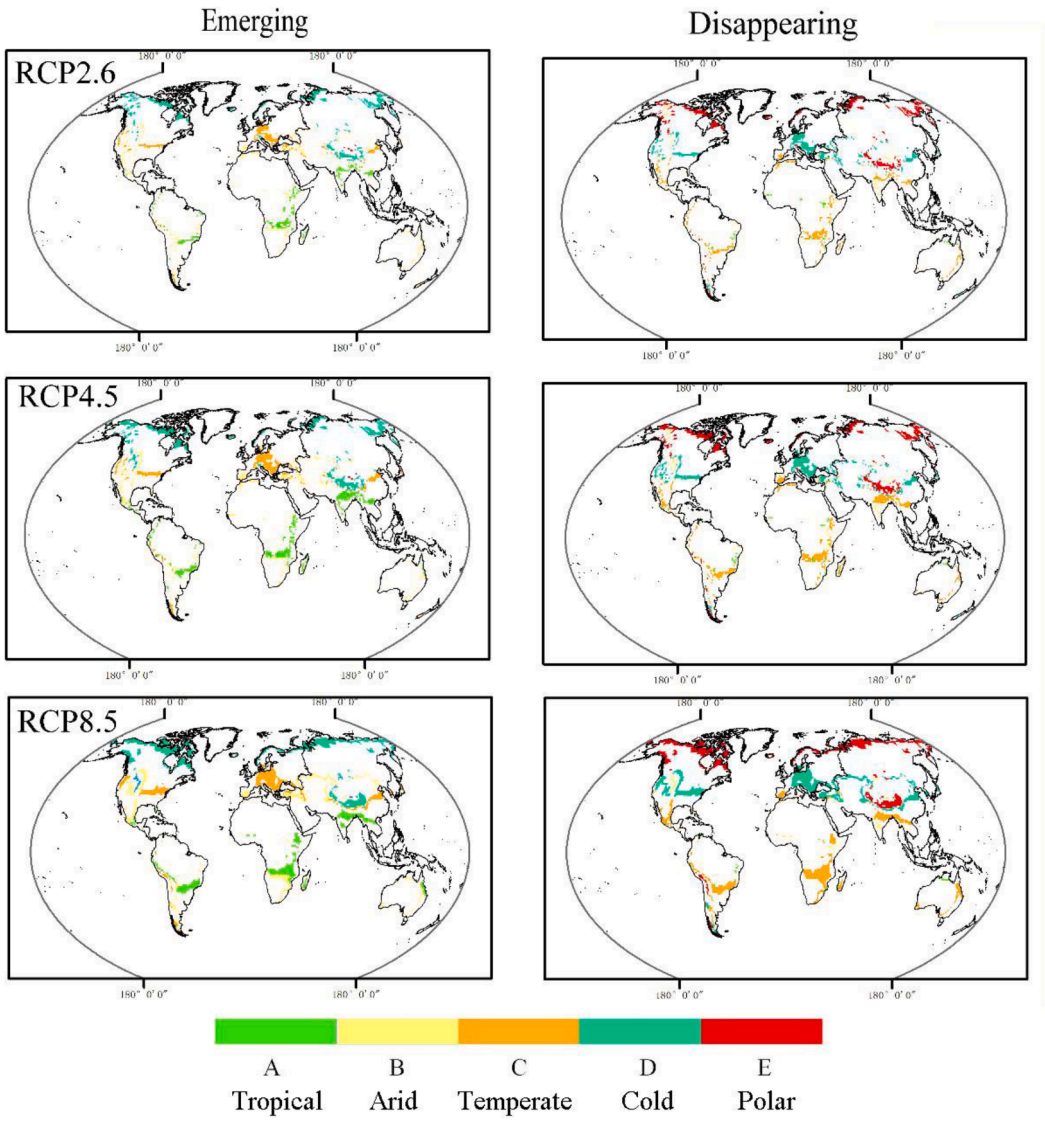

Fig. 1. Distributions of emerging and disappearing Köppen climate zones in the multi-model mean between the period of 1901–1950 and 2051–2095.

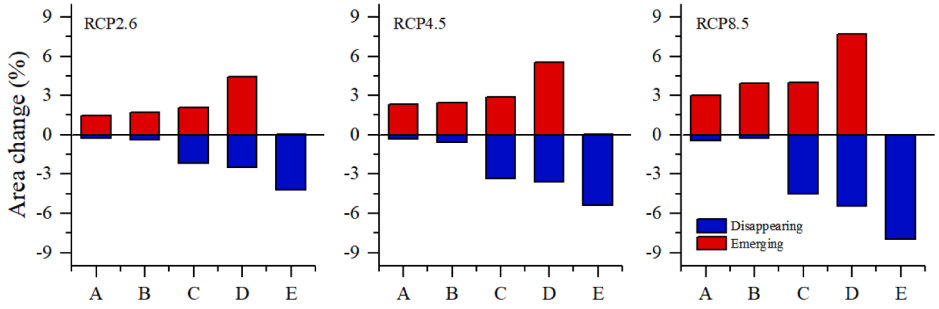

Fig. 2. Area change (%) of Köppen major climate types in the multi-model mean between the period of 1901–1950 and 2051–2095.

3.2. *Changes in global climate heterogeneity*

Figure 3 shows that SHDI decreases at a significance level of 0.01 (MK) under the three emission pathways. Under RCP 2.6, the multi-model mean of SHDI decreases from 1.53 to 1.5 (-0.21×10^{-3}/y) ($p < 0.01$, MK) during 1901–2095. Under RCP 4.5, the downward trends of the multi-model means are further strengthened within the range of 1.53 to 1.47 (-0.32×10^{-3}/y) during the same period. Under RCP 8.5, the multi-model means decrease significantly from 1.53 to 1.46 (-0.41×10^{-3}/y). Overall, as radiative forcing increased from RCP 2.6 to 8.5, the SHDI tended to decrease, suggesting that the higher the emissions, the greater and more rapid the loss of climate heterogeneity.

Figure 4 depicts the spatial distributions of SHDI, showing directional and dispersion changes between the four periods. From RCP 2.6 to 8.5, the SDE coverage of the SHDI tended to decrease (Fig. 4d). Specifically, the SHDI area decreased from 1.9×10^8 km^2 to 1.66×10^8 km^2

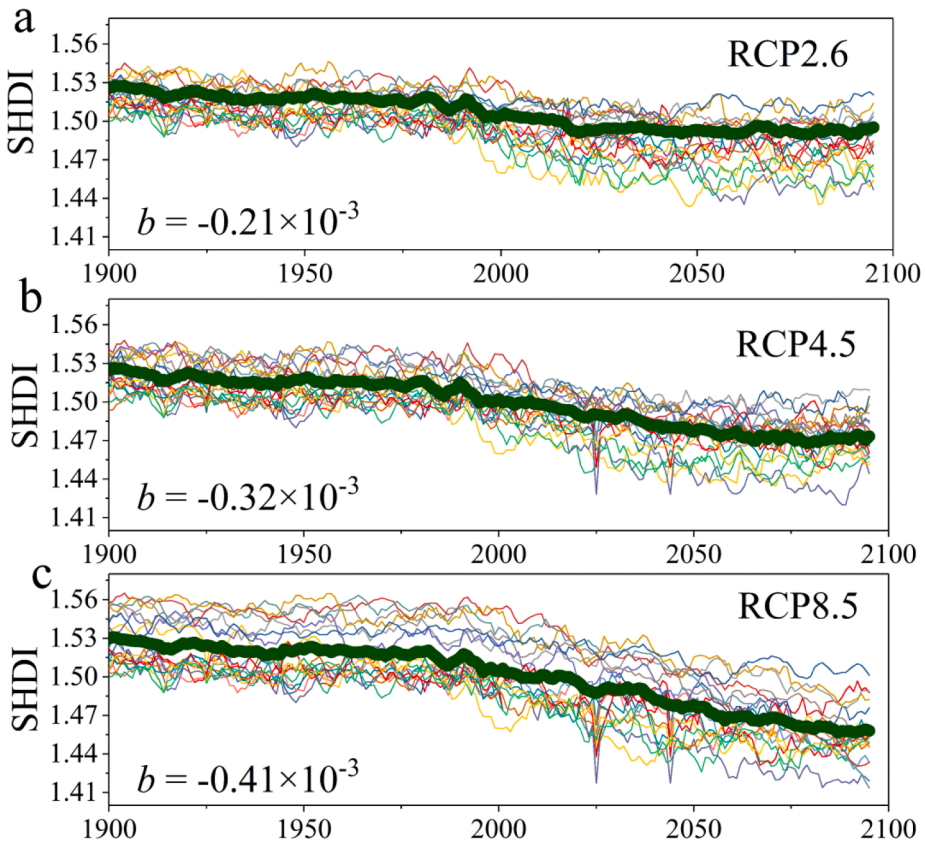

Fig. 3. Dynamics of SHDI under RCP 2.6 (a), 4.5 (b), and 8.5 (c). Dark green line denotes multi-model mean, and coloured lines correspond to different models (Table S1). The temporal trend of each model is statistically significant at the significance level of 0.01 based on the MK test. *b* represents the linear trend of the multi-model mean. (For interpretation of the references to colour in this figure legend, the reader is referred to the web version of this article.)

(RCP 2.6), from 1.977 × 10^8 km^2 to 1.63 × 10^8 km^2 (RCP 4.5), and from 1.945 × 10^8 km^2 to 1.632 × 10^8 km^2 (RCP 8.5). Fig. 4e shows the X-standard distance of the SDE with a pronounced latitudinal trend over the four periods. The SHDI values reduced from 0.429 × 10^6 km to 0.394 × 10^6 km, from 0.44 × 10^6 km to 0.393 × 10^6 km, and from 0.446 × 10^6 km to 0.409 × 10^6 km for RCP 2.6, 4.5, and 8.5, respectively. Overall, by comparing the SDE coverage, directional trend, and X-standard distance over four periods from RCP 2.6 to 8.5, we identified a reduction in the spatial distribution of global climate heterogeneity patterns, with clear latitudinal trends.

3.3. Sensitivity analysis of temperature and precipitation for climate heterogeneity

Figure 5 illustrates the simulated *SHDI* for different climate scenarios, when temperature (*S1*) or precipitation (*S2*) are constant from 1901 to 2095. From RCP 2.6 to 8.5, the minimum, maximum and interquartile range of the simulated *SHDI* for climate scenario (*S2*) are similar to the actual *SHDI* (S0). Specifically, when precipitation is constant, *SHDI* (*S2*) within the range of 1.52 (75th) to 1.499 (25th) for RCP2.6, 1.522 (75th) to 1.493 (25th) for RCP4.5, and 1.521 (75th) to 1.49 (25th) for RCP8.5. In contrast, at constant temperature, *SHDI* (*S1*) change weakly under the three emission pathways. This suggests that temperature is the primary driver in the evolution of global climate heterogeneity under different emission pathways. As radiative forcing intensifies, increasing temperature will have a greater influence on the reduction in global climate heterogeneity than precipitation.

3.4. Attribution of single-forcing experimental simulations to Köppen climate zones

Figure 6 shows the differences in HIST-NAT, HIST-ALL, and HIST-GHG in global climate heterogeneity. In general, the SHDI for anthropogenic forcing (HIST-GHG) and mixed forcing (HIST-ALL) are close to the observed changes during 1940–2000. Specifically, the linear trends decrease at the rates of -0.3×10^{-2} (HIST-GHG), -0.1×10^{-2} (HIST-ALL), and -0.2×10^{-2} (CRU). However, under the HIST-NAT simulation, it is difficult to reproduce the observed changes (CRU) at the rates of 0.4×10^{-4} (SHDI). This suggests that anthropogenic activities and emissions are the main driving forces in the dynamics of global climate heterogeneity.

3.5. Uncertainty analysis of global climate heterogeneity

Figure 7 shows that the internal consistencies of all models are generally stable. From RCP 2.6 to 8.5, the Cronbach alpha (α) coefficients are 0.977, 0.986, and 0.989 for SHDI. As radiative forcing strengthens, the coefficients increase, as does the overall homogeneity or consistency of the models. Upon visual inspection, the lengths of the whiskers for each model from RCP 2.6 to 8.5 are generally larger than those of the multi-model means, indicating that the multi-model mean effectively filters out natural variability and can better simulate changes in global climate heterogeneity. Furthermore, for RCP 2.6, 4.5, and 8.5, the whisker-and-box lengths among all models tend to increase, indicating that the uncertainty for high emissions pathways is greater than that for low emissions pathways. In general, the uncertainties of models in simulating the SHDI are quite large and cover a range of different-paced changes. However, all the models simulate a consistent and downward trend from RCP 2.6 to 8.5.

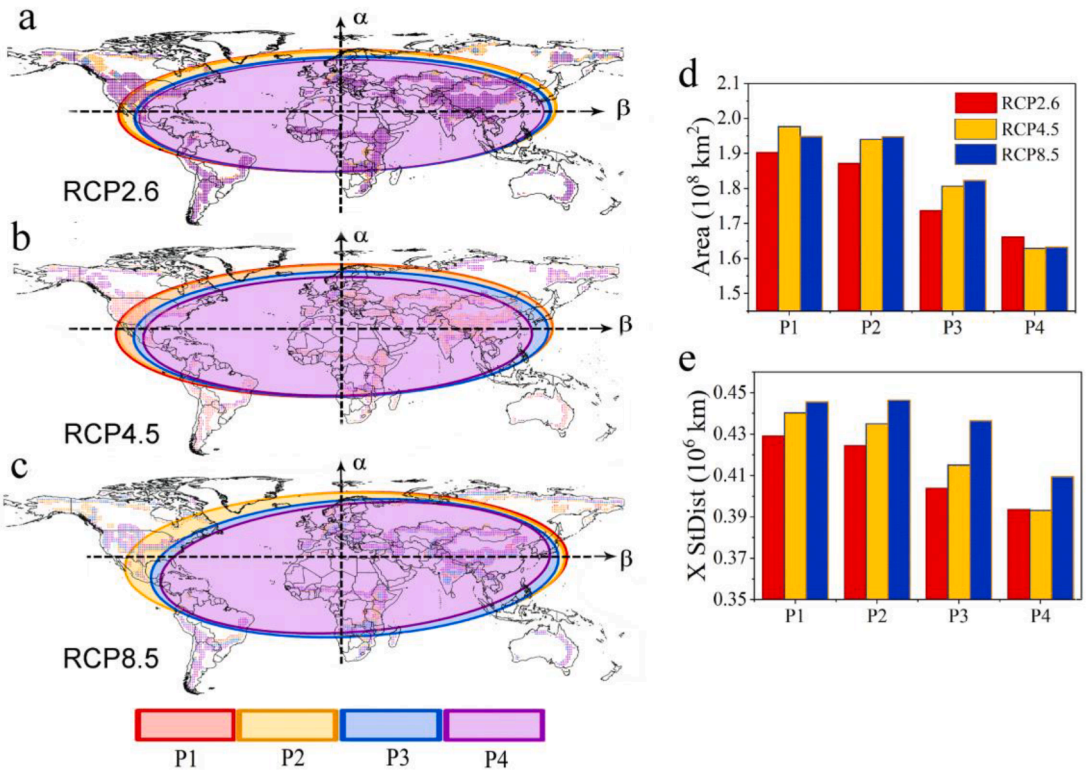

Fig. 4. Spatial distributions (a-c) of SHDI (dots) under RCP 2.6 to 8.5 over four periods. Colour bars denote area change (d) and X-standard distance (e) under RCP2.6 to 8.5 over four periods. α and β represent the directional trends and range of spatial distribution, respectively. P1-P4 denotes the multi-model mean of 1901–1950, 1951–2000, 2001–2050, and 2051–2095.

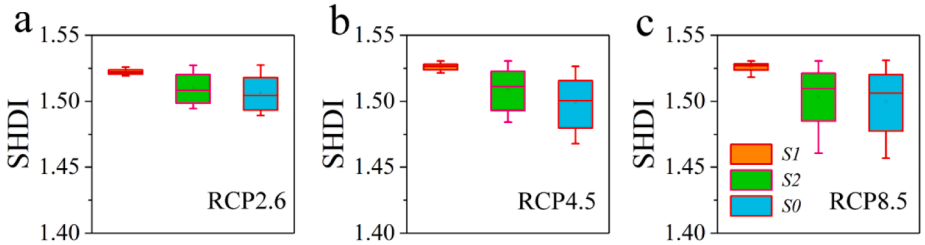

Fig. 5. Sensitivity analysis of SHDI when temperature (*S1*) or precipitation (*S2*) are constant. *S0* denotes actual SHDI. Whisker denotes the Min-Max range and the top and bottom of the boxplots indicate the 75th and 25th percentiles, respectively.

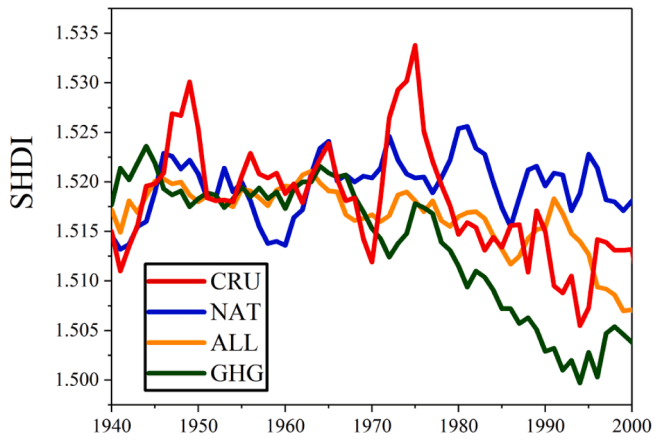

Fig. 6. Dynamics of SHDI for HIST-NAT, HIST-GHG, and HIST-ALL. Except HIST-NAT, the temporal trends decrease at the significance of 0.01 (MK).

4. Discussion

As an important indicator of vegetation coverage, the Köppen climate scheme is widely used in many applications, such as ecological models and climate change impact assessments. Recent studies have shown that simple indicators of climate change can be used to effectively quantify and explain the potential impacts on biodiversity (Garcia et al., 2014; Carroll et al., 2018). Loarie et al. (2009) used the velocity of the climate change index to indicate that high velocities of the climates are only 8% of global protected areas with stability times exceeding 100 years. Burrows et al. (2011), using shifting isotherms, revealed that climate change leads organisms to move and adapt to new climatic types by shifting their biogeographic ranges and changing their phenology. Sunday et al. (2012) reported a phenomenon of global species redistribution due to thermal tolerance. On one hand, factors such as wind and sunlight are not considered in the Köppen–Geiger classification, but may affect the relationship between climate types and vegetation. On the other hand, owing to the inertness of modern ecosystems to climate change (Zhao et al., 2015), the threshold range of precipitation or temperature in response to different vegetation types could be more

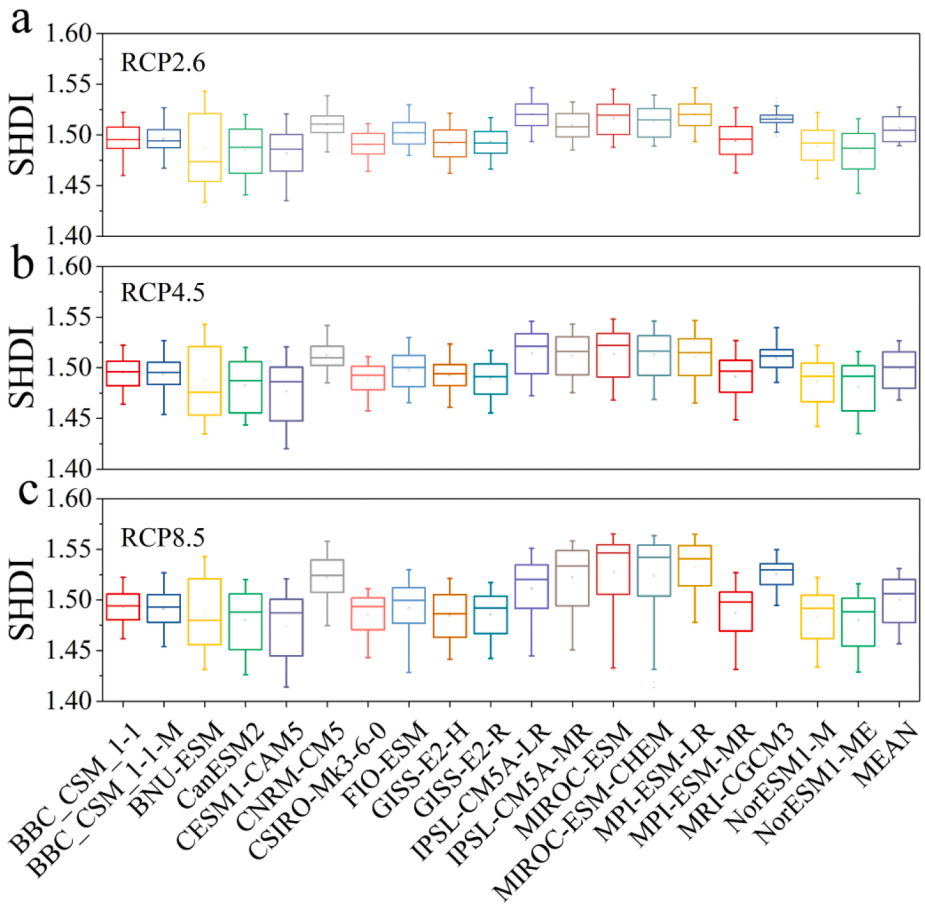

Fig. 7. Box-and-whisker plots (lower sections) for all models. The top and bottom of the boxplots indicate the 75th and 25th percentiles, respectively. Whisker denotes the Min-Max range. As the radiative forcing increases from RCP 2.6 to 8.5, the biases and uncertainty of the models increase.

stable than that of the Köppen climate type. Despite these limitations, the Köppen climate scheme provides a readily computed hydrothermal combination index to explain potential ecological implications. The strong correspondence between the boundaries of Köppen climatic types and biomes indicates that the decrease in climate heterogeneity should be an important means for characterising global biodiversity loss.

Our results reveal the dynamics of global climate heterogeneity from a spatial morphological perspective. Based on landscape indices, we demonstrated that the SHDI of global climatic landscape patterns tended to decrease from 1901 to 2095. Recent research has shown that, by exploring their varying boundaries, it is possible to diagnose or predict substantial changes in present and future climates (Mahlstein et al., 2013; Feng et al., 2014; Beck et al., 2018). Earlier studies considered variations in climate type areas at different scales or the rate at which these shifts occur. However, they did not consider that these changes will cause certain regions to be recategorised as different climate types; however, the overall proportion of these climate types may not change on a larger spatial scale. From a spatial morphological perspective, these moving boundaries will inevitably cause spatial structural (such as patch aggregation) or functional changes (such as heterogeneity) in the global climatic landscape pattern. However, it should be noted that the morphological changes at the global and regional scales are not necessarily consistent (Guan et al., 2020). Despite these limitations, the measurement of climatic morphology deepens our understanding of the heterogeneity of climate itself.

Our results further indicate that the spatial distribution of global SHDI patterns tends to correlate with clear latitudinal trends. Similar to poleward movements in earlier research (Lu et al., 2009; Burrows et al., 2011; Mahlstein et al., 2013; Chan and Wu, 2015), this phenomenon can be attributed to temperature playing a more significant role than precipitation in the variations in global climate heterogeneity. However, this study focuses on climate change on a horizontal scale, and some important factors, such as changes in the vertical scale, have not been considered. Some studies have revealed accelerating upward ecological trends that occur in the topographical gradients of mountain regions in response to climate change. For example, accelerating tree line shifts (Cazzolla Gatti et al., 2019) in the Altai Mountains and plant species richness (Bjorkman et al., 2018) across European mountain regions have been linked to a warming climate. This suggests that a more in-depth investigation of the topographical gradient of climate heterogeneity in the future will provide important insights.

An increasing demand placed on today's models is to provide more information on finer spatial resolutions. In many studies related to the Köppen–Geiger climate classification (Wang and Overland, 2004; Peel et al., 2007; Rubel and Kottek, 2010; Belda et al., 2014; Feng et al., 2014; Chan and Wu, 2015; Rohli et al., 2015; Djamila and Yong, 2016; Chen et al., 2017; Rubel et al., 2017), simulated and observed datasets at 0.5, 1.0, and 2.5° resolutions from different research units were frequently used to analyse changes in large-scale climate types. These datasets effectively promoted an understanding of climate type. However, the appropriate spatial resolution should depend on the issues raised and the phenomena considered, as statistical relationships may change with spatial resolution. Furthermore, it is necessary to explore climate heterogeneity on a regional scale. Similar or opposite trends provide a deeper understanding of climate change. It is generally considered that regional factors, such as topography and atmospheric circulation, can affect climate type and distribution on a regional scale.

Although the reorganisation, loss, and increase of species are closely

related to the intensity of changes in climate heterogeneity, it should be noted that these changes are not equivalent to those in actual biomes (Guan et al., 2020). Because the climate sensitivity encapsulated by different GCMs (Ahlström et al., 2013) covers a range of different changes, the global average warming caused by the increase in atmospheric CO_2 concentration will vary in climate models, depending on the assumed intensity and sign of feedbacks that may suppress or amplify the direct radiative forcing of CO_2 through the greenhouse effect (Knutti and Hegerl, 2008). Although different GCMs offer the possibility of exploring future changes in global climate heterogeneity under different emission intensities (Taylor et al., 2012), many current GCMs do not fully explain the impact of anthropogenic CO_2 emissions stored in both the terrestrial biosphere and surface layers of the oceans on future climate change (Le Quéré et al., 2009). We should pay attention to future climate uncertainties induced by the climate sensitivity of different GCMs.

5. Conclusions

In this study, we investigated the dynamics of global climate heterogeneity based on the Köppen climate scheme. As the areas changed substantially in major climate zones under the three warming scenarios, we detected a significant decrease in global climate heterogeneity from 1901 to 2095 at a significance level of 0.01 (MK). As radiative forcing intensified, the trends of heterogeneity loss strengthened. For RCP 2.6, 4.5, and 8.5, the SHDI of the multi-model mean decreased at rates of -0.2×10^{-3}/y, -0.3×10^{-3}/y, and -0.4×10^{-3}/y. In addition, the spatial distributions of SHDI calculated by the moving window method were reduced, and the coverage and X-standard distance of the SDE were reduced significantly, especially for RCP 8.5. Our sensitivity analysis further showed that anthropogenically driven temperature increases, rather than precipitation changes, resulted in the loss of global climate heterogeneity. Our results suggest that, owing to strong spatial overlap, changes in climate heterogeneity are useful for interpreting the impacts of climate change on biomes, such as future biodiversity loss.

6. Availability of data

The data that support the findings are available from the corresponding authors upon request.

Funding

This research is supported by the National Key Research and Development Program of China (Grant No. 2019YFC0507801), the Second Tibetan Plateau Scientific Expedition and Research Program (STEP) (Grant No. 2019QZKK1003), the National Natural Science Foundation of China (Grant No. 41890824), the Strategic Priority Research Program of the Chinese Academy of Sciences (Grant No. XDA20040301) and the CAS Interdisciplinary Innovation Team (Grant No. JCTD-2019-04).

CRediT authorship contribution statement

Yanlong Guan: Methodology, Writing - original draft. **Hongwei Lu:** Conceptualization, Data curation. **Yelin Jiang:** . **Peipei Tian:** Supervision. **Lihua Qiu:** Supervision. **Petri Pellikka:** Writing - review & editing. **Janne Heiskanen:** Writing - review & editing.

Declaration of Competing Interest

The authors declare that they have no known competing financial interests or personal relationships that could have appeared to influence the work reported in this paper.

Acknowledgments

We acknowledge the World Climate Research Programme's Working Group on Coupled Modelling and the climate modelling groups for producing and making available CMIP5 model data sets (https://esgf-node.llnl.gov/search/cmip5/). We also thank Climatic Research Unit (CRU) at the University of East Anglia for providing observational data sets (https://crudata.uea.ac.uk/cru/data/hrg/). We thank Dr. Olga Hannonen for her valuable comments on the manuscript. We also thank anonymous reviewers for their very careful comments.

Appendix A. Supplementary data

Supplementary data to this article can be found online at https://doi.org/10.1016/j.ecolind.2021.108075.

References

Ahlström, A., Smith, B., Lindström, J., Rummukainen, M., Uvo, C.B., 2013. GCM characteristics explain the majority of uncertainty in projected 21st century terrestrial ecosystem carbon balance. Biogeosciences 10 (3), 1517–1528. https://doi.org/10.5194/bg-10-1517-201310.5194/bg-10-1517-2013-supplement.

Beaumont, L.J., Pitman, A., Perkins, S., Zimmermann, N.E., Yoccoz, N.G., Thuiller, W., 2011. Impacts of climate change on the world's most exceptional ecoregions. Proc. Natl. Acad. Sci. USA 108 (6), 2306–2311. https://doi.org/10.1073/pnas.1007217108.

Beck, H.E., Zimmermann, N.E., McVicar, T.R., Vergopolan, N., Berg, A., Wood, E.F., 2018. Present and future köppen-geiger climate classification maps at 1-km resolution. Sci. Data 5 (1). https://doi.org/10.1038/sdata.2018.214.

Belda, M., Holtanová, E., Halenka, T., Kalvová, J., 2014. Climate classification revisited: from Köppen to Trewartha. Clim. Res. 59 (1), 1–13. https://doi.org/10.3354/cr01204.

Bjorkman, A.D., Pauli, H., Normand, S., et al. (2018) Accelerated increase in plant species richness on mountain summits is linked to warming. Nature 556, 231–234. doi: 10.1038/s41586-018-0005-6.

Bonett, D.G., Wright, T.A., 2015. Cronbach's alpha reliability: Interval estimation, hypothesis testing, and sample size planning. J. Organ. Behav. 36 (1), 3–15. https://doi.org/10.1002/job.1960.

Burrows, M.T., Schoeman, D.S., Buckley, L.B., et al (2011) The pace of shifting climate in marine and terrestrial ecosystems. Science (80-) 334, 652–655. doi: 10.1126/science.1210288.

Carroll, C., Parks, S.A., Dobrowski, S.Z., Roberts, D.R., 2018. Climatic, topographic, and anthropogenic factors determine connectivity between current and future climate analogs in North America. Glob. Chang. Biol. 24 (11), 5318–5331. https://doi.org/10.1111/gcb.2018.24.issue-1110.1111/gcb.14373.

Cazzolla Gatti, R., Callaghan, T., Velichevskaya, A., Dudko, A., Fabbio, L., Battipaglia, G., Liang, J., 2019. Accelerating upward treeline shift in the Altai Mountains under last-century climate change. Sci. Rep. 9 (1) https://doi.org/10.1038/s41598-019-44188-1.

Chan, D., Wu, Q., 2015. Significant anthropogenic-induced changes of climate classes since 1950. Sci. Rep. 5, 1–8. https://doi.org/10.1038/srep13487.

Chan, D., Wu, Q., Jiang, G., Dai, X., 2016. Projected shifts in Köppen climate zones over China and their temporal evolution in CMIP5 multi-model simulations. Adv. Atmos. Sci. 33 (3), 283–293. https://doi.org/10.1007/s00376-015-5077-8.

Chen, T., Zhang, H., Chen, X., Hagan, D.F., Wang, G., Gao, Z., Shi, T., 2017. Robust drying and wetting trends found in regions over China based on Köppen climate classifications. J. Geophys. Res. 122 (8), 4228–4237. https://doi.org/10.1002/2016JD026168.

Deutsch, C.A., Tewksbury, J.J., Huey, R.B., Sheldon, K.S., Ghalambor, C.K., Haak, D.C., Martin, P.R., 2008. Impacts of climate warming on terrestrial ectotherms across latitude. Proc. Natl. Acad. Sci. USA 105 (18), 6668–6672. https://doi.org/10.1073/pnas.0709472105.

Djamila, H., Yong, T.L., 2016. A study of Köppen-Geiger system for comfort temperature prediction in Melbourne city. Sustain. Cities Soc. 27, 42–48. https://doi.org/10.1016/j.scs.2016.08.009.

Elsen, P.R., Monahan, W.B., Merenlender, A.M., 2018. Global patterns of protection of elevational gradients in mountain ranges. Proc. Natl. Acad. Sci. 115 (23), 6004–6009. https://doi.org/10.1073/pnas.1720141115.

Feddema, J.J., 2005. A revised thornthwaite-type global climate classification. Phys. Geogr. 26 (6), 442–466. https://doi.org/10.2747/0272-3646.26.6.442.

Feng, S., Ho, C.-H., Hu, Q., Oglesby, R.J., Jeong, S.-J., Kim, B.-M., 2012. Evaluating observed and projected future climate changes for the Arctic using the Köppen-Trewartha climate classification. Clim. Dyn. 38 (7-8), 1359–1373. https://doi.org/10.1007/s00382-011-1020-6.

Feng, S., Hu, Q., Huang, W., Ho, C.-H., Li, R., Tang, Z., 2014. Projected climate regime shift under future global warming from multi-model, multi-scenario CMIP5 simulations. Glob. Planet Change 112, 41–52. https://doi.org/10.1016/j.gloplacha.2013.11.002.

Garcia, R.A., Cabeza, M., Rahbek, C., Araújo, M.B. (2014) Multiple dimensions of climate change and their implications for biodiversity. Science (80-) 344, 1247579–1247579. doi: 10.1126/science.1247579.

Gaston, K.J., 2000. Global patterns in biodiversity. Nature 405 (6783), 220–227.
Guan, Y., Lu, H., He, L.i., Adhikari, H., Pellikka, P., Maeda, E., Heiskanen, J., 2020. Intensification of the dispersion of the global climatic landscape and its potential as a new climate change indicator. Environ. Res. Lett. 15 (11), 114032. https://doi.org/10.1088/1748-9326/aba2a7.
Guisan, A., Zimmermann, N.E., 2000. Predictive habitat distribution models in ecology. Ecol. Modell. 135 (2-3), 147–186. https://doi.org/10.1016/S0304-3800(00)00354-9.
Kendall, M.G., 1975. Rank Correlation Methods. Griffin, London.
Knutti, R., Hegerl, G.C., 2008. The equilibrium sensitivity of the Earth's temperature to radiation changes. Nat. Geosci. 1 (11), 735–743. https://doi.org/10.1038/ngeo337.
Kottek, M., Grieser, J., Beck, C., Rudolf, B., Rubel, F., 2006. World map of the Köppen-Geiger climate classification updated. Meteorol. Zeitschrift 15 (3), 259–263. https://doi.org/10.1127/0941-2948/2006/0130.
Le Quéré, C., Raupach, M.R., Canadell, J.G., Marland, G., Bopp, L., Ciais, P., Conway, T. J., Doney, S.C., Feely, R.A., Foster, P., Friedlingstein, P., Gurney, K., Houghton, R.A., House, J.I., Huntingford, C., Levy, P.E., Lomas, M.R., Majkut, J., Metzl, N., Ometto, J.P., Peters, G.P., Prentice, I.C., Randerson, J.T., Running, S.W., Sarmiento, J.L., Schuster, U., Sitch, S., Takahashi, T., Viovy, N., van der Werf, G.R., Woodward, F.I., 2009. Trends in the sources and sinks of carbon dioxide. Nat. Geosci. 2 (12), 831–836. https://doi.org/10.1038/ngeo689.
Lee, J., 1947. Determination of world plant formations from simple climatic data. Science (80-) 105 (2727), 367–368.
Loarie, S.R., Duffy, P.B., Hamilton, H., Asner, G.P., Field, C.B., Ackerly, D.D., 2009. The velocity of climate change. Nature 462 (7276), 1052–1055. https://doi.org/10.1038/nature08649.
Lu, H., Guan, Y., He, L., Adhikari, H., Pellikka, P., Heiskanen, J., Maeda, E., 2020. Patch aggregation trends of the global climate landscape under future global warming scenario. Int. J. Climatol. 40 (5), 2674–2685. https://doi.org/10.1002/joc.v40.510.1002/joc.6358.
Lu, J., Deser, C., Reichler, T., 2009. Cause of the widening of the tropical belt since 1958. Geophys. Res. Lett. 36, 3–7. https://doi.org/10.1029/2008GL036076.
Mahlstein, I., Daniel, J.S., Solomon, S., 2013. Pace of shifts in climate regions increases with global temperature. Nat. Clim. Chang. 3 (8), 739–743. https://doi.org/10.1038/nclimate1876.
Mahony, C.R., Cannon, A.J., 2018. Wetter summers can intensify departures from natural variability in a warming climate. Nat. Commun. 9 (1) https://doi.org/10.1038/s41467-018-03132-z.
McGarigal, K., Cushman, S.A., Neel, M.C., Ene, E. (2002) FRAGSTATS: Spatial Pattern Analysis Program for Categorical Maps. 1–182. doi: 10.1016/S0022-3913(12)00047-9.
Mann, H.B., 1945. Nonparametric tests against trend. Econom. J. Econom. Soc. 13, 245–259.
Niskanen, A.K.J., Heikkinen, R.K., Mod, H.K., Väre, H., Luoto, M., 2017. Improving forecasts of arctic-alpine refugia persistence with landscape-scale variables. Geogr. Ann. Ser. A Phys. Geogr. 99 (1), 2–14. https://doi.org/10.1080/04353676.2016.1256746.
Ohlemüller, R., Anderson, B.J., Araújo, M.B., Butchart, S.H.M., Kudrna, O., Ridgely, R.S., Thomas, C.D., 2008. The coincidence of climatic and species rarity: High risk to small-range species from climate change. Biol. Lett. 4 (5), 568–572. https://doi.org/10.1098/rsbl.2008.0097.
Peel, M.C., Finlayson, B.L., McMahon, T.A., 2007. Updated world map of the Köppen-Geiger climate classification. Hydrol. Earth Syst. Sci. 11 (5), 1633–1644. https://doi.org/10.5194/hess-11-1633-2007.
Pickett, A.S.T.A., Cadenasso, M.L., 1995. Landscape ecology: spatial heterogeneity in ecological systems. Science (80-) 269, 331–334.
Rohli, R.V., Andrew Joyner, T., Reynolds, S.J., et al., 2015. Globally Extended Kppen-Geiger climate classification and temporal shifts in terrestrial climatic types. Phys. Geogr. 36, 142–157. https://doi.org/10.1080/02723646.2015.1016382.
Rubel, F., Brugger, K., Haslinger, K., Auer, I., 2017. The climate of the European Alps: shift of very high resolution Köppen-Geiger climate zones 1800–2100. Meteorol. Zeitschrift 26 (2), 115–125. https://doi.org/10.1127/metz/2016/0816.
Rubel, F., Kottek, M., 2010. Observed and projected climate shifts 1901–2100 depicted by world maps of the Köppen-Geiger climate classification. Meteorol. Zeitschrift 19 (2), 135–141. https://doi.org/10.1127/0941-2948/2010/0430.
Schwalm, C.R., Anderegg, W.R.L., Michalak, A.M., Fisher, J.B., Biondi, F., Koch, G., Litvak, M., Ogle, K., Shaw, J.D., Wolf, A., Huntzinger, D.N., Schaefer, K., Cook, R., Wei, Y., Fang, Y., Hayes, D., Huang, M., Jain, A., Tian, H., 2017. Global patterns of drought recovery. Nature 548 (7666), 202–205. https://doi.org/10.1038/nature23021.
Scott, L.M., Janikas, M.V. (2010) Spatial Statistics in ArcGIS. In: Handbook of Applied Spatial Analysis. Springer Berlin Heidelberg, Berlin, Heidelberg, pp 27–41.
Seidel, D.J., Fu, Q., Randel, W.J., Reichler, T.J., 2008. Widening of the tropical belt in a changing climate. Nat. Methods 1 (1), 21–24. https://doi.org/10.1038/ngeo.2007.38.
Shannon, C.E., 1948. A mathematical theory of communication. Bell. Syst. Tech. J. 27, 623–656. https://doi.org/10.1002/j.1538-7305.1948.tb01338.x.
Simpson EH (1949) Measurement of diversity [16]. Nature 163:688. doi: 10.1038/163688a0.
Sunday, J.M., Bates, A.E., Dulvy, N.K., 2012. Thermal tolerance and the global redistribution of animals. Nat. Clim. Chang. 2, 686–690. https://doi.org/10.1038/nclimate1539.
Taylor, K.E., Balaji, V., Hankin, S., et al., 2010. CMIP5 data reference syntax (DRS) and controlled vocabularies. Syntax 1–14.
Taylor, K.E., Stouffer, R.J., Meehl, G.A., 2012. An overview of CMIP5 and the experiment design. Bull. Am. Meteorol. Soc. 93, 485–498. https://doi.org/10.1175/BAMS-D-11-00094.1.
Thornthwaite, C.W., 1961. The task ahead. Ann. Assoc. Am. Geogr. 51, 345–356. https://doi.org/10.1111/j.1467-8306.1979.tb01220.x.
Thornthwaite, C.W., 1948. An approach toward a rational classification of climate. Geogr. Rev. 33, 233–255.
van der Schrier, G., Barichivich, J., Briffa, K.R., Jones, P.D., 2013. A scPDSI-based global data set of dry and wet spells for 1901–2009. J. Geophys. Res. Atmos. 118 (10), 4025–4048. https://doi.org/10.1002/jgrd.50355.
Vicente-Serrano, S.M., Beguería, S., López-Moreno, J.I., et al (2010) A new global 0.5° gridded dataset (1901–2006) of a multiscalar drought index: comparison with current drought index datasets based on the palmer drought severity index. J. Hydrometeorol. 11:1033–1043. doi: 10.1175/2010JHM1224.1.
Wang, M., Overland, J.E., 2004. Detecting arctic climate change using Köppen climate classification. Clim. Change 67, 43–62. https://doi.org/10.1007/s10584-004-4786-2.
Zhang, Y., You, Q., Chen, C., et al (2018) Evaluation of downscaled CMIP5 Coupled with VIC model for flash drought simulation in a humid subtropical basin, China. J Clim 31:1075–1090. doi: 10.1175/JCLI-D-17-0378.1.
Zhao, Y., Herzschuh, U., Li, Q., 2015. Complex vegetation responses to climate change on the Tibetan Plateau: a paleoecological perspective. Natl. Sci. Rev. 2, 400–402. https://doi.org/10.1093/nsr/nwv057.